Applied Physics Letters

Characterizing the electrical breakdown properties of single n-i-n-n^+:GaN nanowires

Cite as: Appl. Phys. Lett. **113**, 193103 (2018); https://doi.org/10.1063/1.5050511
Submitted: 31 July 2018 . Accepted: 22 October 2018 . Published Online: 07 November 2018

Juntian Qu, Renjie Wang, Yu Sun, Ishiang Shih, Zetian Mi, and Xinyu Liu

ARTICLES YOU MAY BE INTERESTED IN

Room-temperature photoluminescence lifetime for the near-band-edge emission of (000 $\bar{1}$) p-type GaN fabricated by sequential ion-implantation of Mg and H
Applied Physics Letters **113**, 191901 (2018); https://doi.org/10.1063/1.5050967

1230 V β-Ga_2O_3 trench Schottky barrier diodes with an ultra-low leakage current of <1 $\mu A/cm^2$
Applied Physics Letters **113**, 202101 (2018); https://doi.org/10.1063/1.5052368

Investigation of GaN-on-GaN vertical p-n diode with regrown p-GaN by metalorganic chemical vapor deposition
Applied Physics Letters **113**, 233502 (2018); https://doi.org/10.1063/1.5052479

© 2018 Author(s).

APPLIED PHYSICS LETTERS **113**, 193103 (2018)

Characterizing the electrical breakdown properties of single n-i-n-n$^+$:GaN nanowires

Juntian Qu,[1,2,a)] Renjie Wang,[3,a)] Yu Sun,[1] Ishiang Shih,[3] Zetian Mi,[3,4,b)] and Xinyu Liu[1,2,b)]
[1]*Department of Mechanical and Industrial Engineering, University of Toronto, Toronto, Ontario M5S 3G8, Canada*
[2]*Department of Mechanical Engineering, McGill University, Montreal, Quebec H3A 0C3, Canada*
[3]*Department of Electrical and Computer Engineering, McGill University, Montreal, Quebec H3A 0E9, Canada*
[4]*Department of Electrical Engineering and Computer Science, University of Michigan, Ann Arbor, Michigan 48109, USA*

(Received 31 July 2018; accepted 22 October 2018; published online 7 November 2018)

The electrical transport properties and breakdown behaviors of single n-i-n-n$^+$ GaN nanowires (NWs) are investigated through *in-situ* nanoprobing inside a scanning electron microscope (SEM). The nanoprobing contact resistance is dramatically reduced by increasing the Si-doping concentration of the top n$^+$-GaN segment of the NW. The dependence of the NW breakdown parameters (i.e., breakdown voltage, power, and current density) on the n$^+$-GaN Si-doping concentration and the NW diameter is experimentally quantified and explained by the localized thermal decomposition mechanism of the NW. Enabled by the low NW-nanoprobe contact resistance, a breakdown current density of 4.65 MA/cm^2 and a breakdown power of 96.84 mW are achieved, both the highest among the previously reported results measured on GaN NWs. *Published by AIP Publishing.*
https://doi.org/10.1063/1.5050511

Recent advances in microelectronics have made group III-nitride nanowires (NWs) in the spotlight owing to the excellent controllability of their electronic properties[1] and their broad applications in (opto)electronics.[2] Catalyst-free gallium nitride (GaN) NWs, usually vertically grown on a substrate by molecular beam epitaxy (MBE), possess high crystalline quality (e.g., strain- and dislocation-free) and high electron mobilities, and thus hold great potential for use in high-power and/or high-frequency electronic devices.[2,3]

The electrical properties (e.g., transport property and breakdown behavior) of GaN NWs significantly affect the performance of GaN-NW-based devices. As an important electrical property, the breakdown current density of GaN NWs has been studied previously. Due to Joule heating, the breakdown of horizontally arranged GaN NWs has been observed to occur at an average current density of approximately 3×10^6 A/cm^2 at estimated peak temperatures of around 1050–1100 K.[4,5] However, due to phonon surface scattering, the relatively poor heat dissipation of NWs has hindered the development of high performance vertically oriented GaN NW devices.[6,7] The level of breakdown current density of GaN NWs tends to depend on NW geometries (e.g., diameter and height), material compositions, and arrangements on their growth substrates. Recently, GaN-NW arrays with precisely controlled geometries, composition, and array pattern arrangement have been synthesized by using selective area epitaxy (SAE),[8–12] and these GaN-NW arrays have been used to fabricate a variety of optoelectronic devices such as multi-color light emitting devices (LEDs) and full-color displays.[11–13]

The GaN NWs are typically grown on sapphire substrates with thick GaN epilayers.[10–12] Compared to sapphire substrates, heavily doped Si substrates exhibit advantages of high thermal and electrical conductivities, and thus can serve as a good heat sink at the NW bottom for high-power electronic applications. To be compatible with existing silicon device technologies, SAE of GaN NWs on a Si substrate has been recently explored and investigated by many researchers.[14–16] In this work, we synthesized high-quality n-i-n-n$^+$ GaN NWs on a Si substrate using SAE, and obtained SAE NWs with different diameters on the same Si substrate. This allows us to readily perform electrical nanoprobing on as-grown GaN NWs, and study the effect of the NW diameter and doping level on the electrical breakdown behavior of the NWs.

This paper reports the electrical characterization of single n-i-n-n$^+$ GaN NWs vertically grown on a Si substrate through SAE. Benefiting from the flexibility of the *in-situ* nanoprobing technique inside a scanning electron microscope (SEM), the electrical breakdown parameters (i.e., breakdown voltage, power, and current density) of the n-i-n-n$^+$ GaN NWs were experimentally quantified, and the dependence of the NW breakdown behavior on the NW diameter and the Si-doping concentration of the top n$^+$-GaN segment of the NW was investigated. Leveraging the excellent transport property of the n-i-n-n$^+$ NW structure and the low NW-nanoprobe contact resistance (enabled by the high Si-doping level of the n$^+$-GaN segment), a breakdown current density of up to 4.65 MA/cm^2 and a breakdown power of up to 96.84 mW were achieved, both the highest among the previously reported breakdown parameters of single GaN NWs. The results will provide useful guidelines for experimentally improving the breakdown performance of single GaN NWs with precisely controlled geometries on Si

[a)]J. Qu and R. Wang contributed equally to this work.
[b)]Authors to whom correspondence should be addressed: xyliu@mie.utoronto.ca, tmi@umich.edu

substrates, and thus enable applications of these GaN NWs in high-power nanoelectronics.

The n-i-n-n$^+$ GaN-NW heterostructures were epitaxially grown on an n-Si substrate (prime grade as-doped Si wafers, Nova Electronic Materials; thickness: $279 \pm 25\,\mu$m), using a radio frequency plasma-assisted MBE system (GENxplor, Veeco). Ti-mask-based SAE was employed to regulate the NW diameter.[8,9,17] The details of the NW growth process are introduced in the supplementary material. As shown in Fig. 1(a), an n-i-n-n$^+$ GaN NW heterostructure consists of segments of $\sim$100 nm lightly Si-doped n-GaN, $\sim$500 nm non-doped GaN, $\sim$100 nm lightly Si-doped n-GaN, and $\sim$100 nm heavily Si-doped n$^+$-GaN (bottom to top). The heavy doping of the n$^+$-GaN segment ensures low resistance between the NW and the subsequently deposited Ti/Au electrode on its top surface.

Figure 1(b) shows a typical SEM photograph of five n-i-n-n$^+$:GaN NWs grown on the same substrate, all with a hexagonal morphology. The maximum diameter of the hexagonal NW cross section (simply called the diameter of the NW in the following paragraphs) of the NW samples ranges from 400 nm to 950 nm, and was controlled by adjusting the size of the Ti nanohole initially patterned on the Si substrate (Ti mask). The capability of readily controlling the NW diameter, enabled by the Ti-mask SAE technique, allows us to characterize the electrical transport properties of the n-i-n-n$^+$ GaN NWs at different NW diameters and, therefore, establish the relationship between the NW diameter/cross-sectional area and the material's electrical breakdown parameters such as breakdown voltage and power.

The crystal quality of the NW was examined through high-resolution transmission electron microscopy (TEM) (FEI Tecnai F20 with a camera of 4000×4000 pixels). Figure 1(c) shows the crystalline structure of the root region of the n-i-n-n$^+$:GaN NW, indicating high crystal quality. The interplane spacing of the NW crystal was measured to be 0.26 nm, confirming the NW growth along the [0002] direction (c-axis). The selected-area electron diffraction (SAED) pattern [inset of Fig. 1(c)] also confirms the [0002] growth direction.

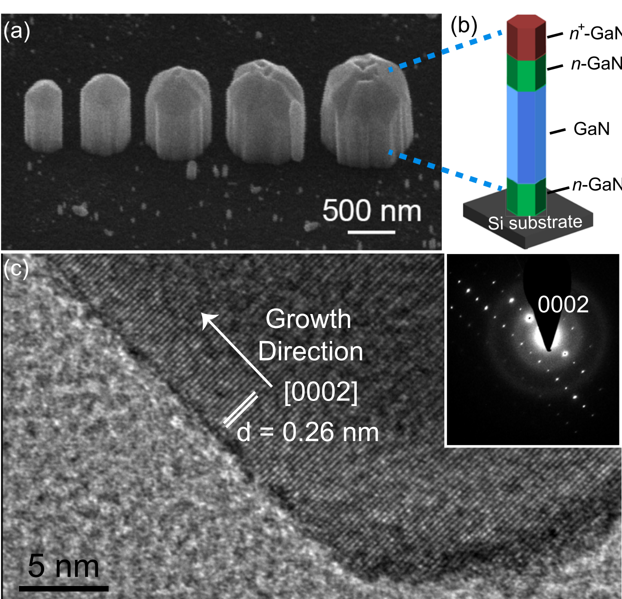

FIG. 1. Sample illustrations: (a) SEM images (45° tilt angle) of single GaN NWs with precisely controlled diameters ranging from 400 to 800 nm. (b) Schematic of single n-i-n-n$^+$:GaN NWs grown on a Si substrate. (c) High-resolution TEM image and selected area electron diffraction (SAED) pattern (inset) of the NW crystal structure.

To improve the electrical contacts between the two nanoprobes and the NW sample, Ti/Au electrodes were deposited on top surfaces of the NWs and on the back side of the Si substrate [Fig. 2(a)] through e-beam deposition. The Ti/Au deposition on top of the n$^+$-GaN segment was based on polyimide-based surface passivation and planarization,[18] and the process details can be found in the supplementary material.

We performed two-point electrical *in-situ* nanoprobing of the as-grown single n-i-n-n$^+$:GaN NWs inside a SEM by following a previously developed protocol.[19] Compared with the conventional nanolithography based techniques for establishing electrical contacts with a single NW,[20] *in-situ* nanoprobing is relatively easy to perform, is more rapid, and allows the testing of many NWs with less experimental efforts for examining the effect of different growth parameters on the material's electrical properties. More importantly, nanolithography for patterning electrodes on a NW involves chemical treatment of the NW that may alter the NW's electrical properties,[20,21] but this is avoided in *in-situ* nanoprobing.

A nanomanipulator (LF-2000, Toronto Nanoinstrumentation Inc.), mounted inside an SEM (Quanta 450 FEG, FEI), was employed for positioning conductive nanoprobes for electrical probing and testing of single NWs. The nanomanipulator integrates position feedback (resolution: 0.1 nm) on each of its fine positioning stage, allowing closed-loop controlled, high-precision nanopositioning. The bottom-right inset of Fig. 2(b) shows an n-i-n-n$^+$:GaN NW being probed by a Pt-coated tungsten nanoprobe (ST-20–0.5, GGB Industries).

In our nanoprobing experiments, one nanoprobe contacts the metal at the top surface of a GaN NW [inset of Fig. 2(b)], and the other one contacts the back electrode on the back side of the Si substrate. The resistance of the Si substrate (resistivity: $0.005\,\Omega\cdot$cm and thickness: $279 \pm 25\,\mu$m) along its thickness was estimated to be $0.00014\,\Omega$, which can be safely ignored compared to the GΩ- to kΩ-level resistance of the NW. A precision source meter (SMU 2400, Keithley) was employed for I-V measurements of the NW samples.

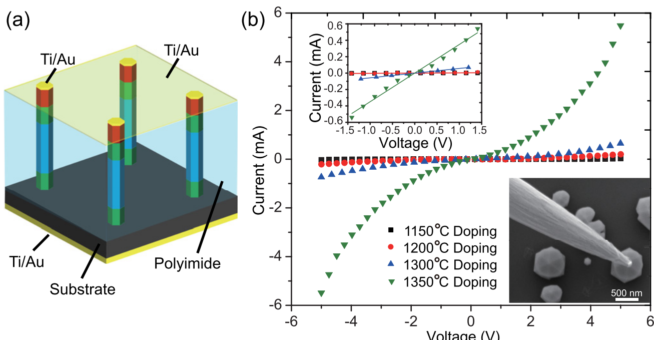

FIG. 2. (a) 3D schematic of GaN single NW devices fabricated on a Si substrate. (b) Representative I-V characteristics of single GaN NWs with different doping levels, obtained by nanoprobing individual GaN NWs with a length of $\sim$800 nm and a diameter of $\sim$500 nm. The top-left inset shows the magnified I-V curves (voltage: -1.5 V to 1.5 V), based on which the NW overall resistance was calculated. The bottom-right inset shows the SEM image of such nanoprobing with a Pt-coated tungsten tip.

The sweeping voltage was from −5 V to 5 V with a step increment of 0.25 V and a ramp rate of 100 V/s. During the measurement, the e-beam radiation from the SEM was switched off using a beam blanker to avoid any electrical noise induced by the incident electrons. In addition, before each measurement, the two nanoprobes connecting the GaN NW sample were first grounded to eliminate any charge built-up on the sample due to SEM imaging.

Figure 2(b) shows the representative I-V curves of single n-i-n-n^+ GaN NWs (height: 800 nm and diameter: 500 nm) with four different doping concentrations in the n^+ segments of the samples. The linear I-V characteristics are observed in the low voltage bias [−1.5 to 1.5 V, top-left inset of Fig. 2(b)] region (ohmic regime), while the nonlinear current voltage characteristics are generally observed in the relatively high voltage bias (−6 to 6 V) region which is a space-charge-limited (SCL) regime for a solid with a relatively low free carrier concentration.[22,23] One can also see that the Si-doping level in the n^+-GaN segment of an n-i-n-n^+ GaN NW significantly affects its I-V characteristics. According to the slopes of the linear regions of the I-V curves in the low sweep voltage range of −1.5 to 1.5 V, the resistance values of individual GaN NW were calculated to be 2 MΩ, 0.5 MΩ, 16 kΩ, and 3.3 kΩ for NWs with Si doping temperatures of 1150 °C, 1200 °C, 1300 °C, and 1350 °C, respectively (n = 5). Based on the resistance equation $R = l/(\sigma \cdot A)$, the overall conductivity values (denoted by σ) of these NWs were calculated to be 0.023 $(\Omega\cdot\text{cm})^{-1}$, 0.092 $(\Omega\cdot\text{cm})^{-1}$, 2.940 $(\Omega\cdot\text{cm})^{-1}$, and 14.255 $(\Omega\cdot\text{cm})^{-1}$ for the Si doping temperatures of 1150 °C, 1200 °C, 1300 °C, and 1350 °C, respectively.

Based on the overall conductivity of a single NW, we estimated the electron density of the intrinsic, non-doped GaN segment of the NW, which is one of the primary parameters of the NW quality. To this end, we used the resistance data measured from n-i-n-n^+ GaN NWs with n^+ segments doped at 1350 °C, which have the lowest contact resistance with the top electrode. Specifically, the electron density value of the non-doped GaN segment was calculated from equation $\sigma = e \cdot n \cdot \mu$,[24] where σ is the conductivity in the non-doped GaN segment, e is the constant value of elemental charge, n is the electron density to be obtained, and μ is the electron mobility for non-doped GaN NWs. A previous study has tested the electron mobility of non-doped GaN NWs to be 650 $\text{cm}^2/(\text{V}\cdot\text{s})$,[1] which was used in our calculation. The corresponding conductivity σ of the non-doped GaN segment was calculated to be 10.11 $(\Omega\cdot\text{cm})^{-1}$ based on the equation $R = l/(\sigma \cdot A)$, where the resistance value R for the non-doped GaN segment was determined to be 3044 Ω (by subtracting the resistance values of the n-GaN and n^+-GaN segments from the total NW resistance of 3.3 kΩ), l is the length of the non-doped GaN segment ($l = 100$ nm), and A is the NW cross-sectional area (diameter: 500 nm). From equation $\sigma = e \cdot n \cdot \mu$, the electron density value of the non-doped GaN segment was finally estimated to be $9.71 \times 10^{16}\,\text{cm}^{-3}$, which is in agreement with the previously reported results of high-quality GaN materials.[1,25]

After the I-V characterization, single n-i-n-n^+ GaN NWs were driven to their electrical breakdown by applying a forward ramp voltage from 0 V to 10 V (with a step increment of 0.25 V and a ramp rate of 100 V/s) at room temperature (21 °C), and the corresponding I-V curves were recorded. When the ramp voltage reached the NW breakdown value, the GaN NW was broken because of the Joule heating effect, and the breakdown voltage of the NW was determined to be the peak value of the I-V curve before the current dropped to zero [Figs. 3(b)–3(e)]. Figures 3(a-1)–3(a-3) show a sequence of three SEM photographs illustrating the process of NW breakdown testing. We also detached two broken NW portions (from two individual tests) onto the same Si substrate for high-magnification SEM imaging. As shown in Fig. 3(a-4), there were Ga nano-balls on the NW portions that were formed from the thermal decomposition of GaN and the subsequent deposition of the decomposed Ga.[4]

The I-V curves for electrical breakdown of single NWs with different diameters (400 nm–900 nm) and Si-doping temperatures (1150 °C–1350 °C) are shown in Figs. 3(b)–3(e). We can see that the current injected through single NW increased with the applied voltage bias until a certain critical point, beyond which the current dramatically dropped to zero. The current and voltage values at the critical point were defined as the breakdown current and voltage. The dependence of the breakdown voltage on the NW diameter and Si-doping level of the n^+-GaN segment is illustrated in Fig. 4(a). Note each data point in Fig. 4(a) is the average of breakdown voltage values measured from three GaN NWs with the same diameter and Si-doping temperature, and the x-axis error reflects the small variation of the NW diameter. The data show that, for the same n^+ doping concentration, the NW breakdown voltage remains relatively constant with small fluctuations (1150 °C doping: 8.51 ± 0.28 V, 1200 °C doping: 8.23 ± 0.52 V, 1300 °C doping: 6.84 ± 0.78 V, and 1350 °C doping: 5.38 ± 0.25 V). The electric field strength at

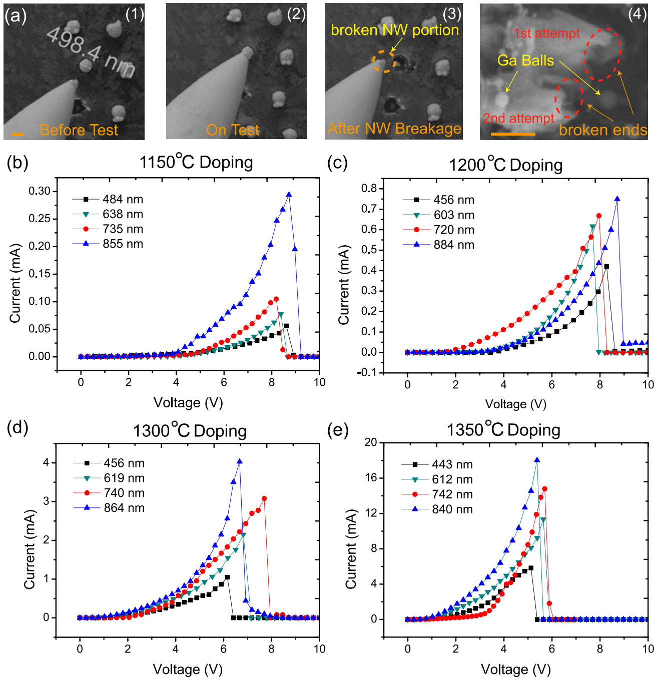

FIG. 3. (a) Sequential SEM images of single GaN NW probing before/on/after breakdown tests (left scale bar: 500 nm) and magnified image (right scale bar: 500 nm) of evaporated Ga balls and the broken NW cross section area of the 1st and the 2nd measurement. (b)–(e) Single GaN NW failure I-V characteristics with different Si doping temperatures used in n^+-GaN: (b) 1150 °C, (c) 1200 °C, (d) 1300 °C, and (e) 1350 °C.

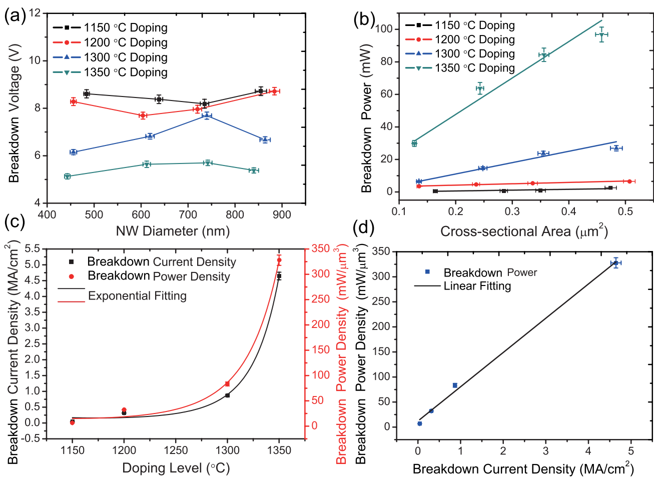

FIG. 4. (a) Doping-dependent breakdown voltage as a function of the NW diameter. (b) Doping-dependent NW breakdown power as a function of the NW cross-sectional area (calculated as regular hexagonal). (c) NW breakdown current density and breakdown power density (red line) as a function of doping temperature (the four data points correspond to the highest current density and power density within four doping temperatures from 1150 °C to 1350 °C). (d) NW breakdown power density as a function of NW current density. n = 3 for all the data.

the NW breakdown was calculated to be in the range of 10.76–17.02 MV/m, which is higher than that (∼4.36 MV/m) measured from single GaN NWs tested in a lateral arrangement.[5] Furthermore, it was observed that, at the same NW diameter, the breakdown voltage decreased when the n^+ doping level increased.

A previous study[5] demonstrated that the electrical breakdown of a GaN NW, which was arranged horizontally inside a TEM, occurred in the middle portion of the NW because the thermal distribution of the NW has the highest temperature (T_{max}) in its middle portion and lower temperatures at its two ends connected with electrodes. In our experimental setup, the Pt-coated tungsten nanoprobe has higher thermal conductivity than that of the Si substrate; thus, the top of the n-i-n-n^+ GaN NW has a lower temperature than that of the NW's root. Assuming constant thermal conductivity over the entire NW, the NW's highest temperature T_{max} is[5,26]

$$T_{max} = T_0 \exp\left(\frac{\alpha \sigma U^2}{8}\right), \tag{1}$$

where α is a constant inversely proportional to the thermal conductivity of the NW, σ is the electrical conductivity of the NW, and U is the applied DC bias (by ignoring the nanoprobe-NW contact resistance). According to Eq. (1), the maximum temperature T_{max} on the NW only depends on the DC bias not the NW diameter.[5] This explains the relatively constant breakdown voltages required to elevate the highest NW temperature (T_{max}) to the material's melting point for NWs with the same Si-doping concentration but different diameters [Fig. 4(a)]. In addition, a higher Si-doping concentration resulted in a larger electrical conductivity (σ) of the NW; this led to the decrease in the breakdown voltage U for NWs with the same diameter [Fig. 4(a)] when the Si-concentration increased, assuming T_{max} is the same for all the NWs. Note that Eq. (1) does not consider the heat transfer efficiency at the top and bottom of a NW and was only used to qualitatively explain the observed trends of the breakdown voltage vs. the Si-doping level and the NW diameter.

Figure 4(b) shows the dependence of the NW breakdown power P (the product of the breakdown voltage and current) on the NW diameter and the n^+-doping level. One can observe that for each Si-doping concentration, the NW breakdown power is linearly proportional to the NW cross-sectional area. For the same cross-sectional area, the NW breakdown power increases with the doping concentration.

Fitting $R = l/(\sigma \cdot A)$ and the power equation $P = U^2/R$ into Eq. (1) yields

$$T_{max} = T_0 \exp\left(\frac{\alpha P l}{8A}\right). \tag{2}$$

From Eq. (2), we can find that the breakdown power (the P value required to drive T_{max} on the NW to reach its melting temperature) is linearly proportional to the NW cross-sectional area (A).

With the same NW cross-sectional area, the higher the Si-doping concentration (thus α) becomes the higher the breakdown power is. Based on Fig. 4(b), the maximum DC power in a single GaN NW (diameter: 840 nm; Si-doping temperature: 1350 °C) is 96.84 mW, which is comparable to the result reported in Ref. 4.

In addition, the dependence of NW breakdown current density on the NW diameter is presented in Fig. S1, showing a slight increase in the value of breakdown current density with a decreased NW diameter at certain Si-doping temperature; as further interpretation, as shown in Fig. 4(c), the NW breakdown current density increases exponentially with the Si-doping temperature. This is primarily due to the fact that the contact resistance between the top electrode and the n^+-GaN segment decreases with the Si-doping concentration,[27] and that the Si-doping concentration is in an exponential relationship with the Si-doping temperature.[27,28] The maximum current density we have achieved was 4.65 MA/cm^2 (current: 11.3 mA, NW diameter: 612 nm, and Si-doping temperature: 1350 °C), which is over 76 times higher than that (0.06 MA/cm^2) of GaN NWs (current: 244 μA and diameter: 800 nm) reported in Ref. 4. Due to the relatively constant breakdown voltages shown in Fig. 4(a) for the same n^+ Si-doping concentration, the corresponding NW breakdown power density (red line) also increases exponentially with the Si-doping temperature, and the maximum power density we have achieved was 327.84 $mW/\mu m^3$. As shown in Fig. 4(d), the NW breakdown power density is linearly proportional to the breakdown current density.

The attained ultrahigh NW breakdown power and current density data demonstrate the merits of the unique n-i-n-n^+ heterostructure of the GaN NW and the effectiveness of Si-doping approach (for the top n^+ segment) to reduce the contact resistance of the NW top surface. One can dramatically increase the breakdown current density and the breakdown power of an n-i-n-n^+ GaN NW by increasing the Si-doping level of the n^+ segment. This illustrates an easy experimental approach for tuning these important electrical parameters of GaN NWs, to improve the performance of GaN-NW-based electronic devices. Note that heat sinks at

the top and bottom of a GaN NW also significantly affect its electrical breakdown properties. In a practical (opto)electronic device involving vertically grown GaN NWs, the heat transfer efficiency at the top and bottom of a NW can be significantly improved by adopting a bottom substrate and a top packaging material both with high thermal conductivity, which will further extend the electrical breakdown limit of the GaN NWs. Moreover, for wire interconnects in modern integrated circuit (ICs), the contact resistance problem also exists,[29,30] and the high contact resistance can cause substantial heating in a high-current IC device. The n^+-segment doping method we demonstrated could potentially mitigate the contact resistance issue in wire interconnects of modern ICs, improving device performance in high-current-density operations.[31,32]

In conclusion, the electrical properties of single n-i-n-n^+ GaN NWs grown on Si substrates were investigated through *in-situ* two-point nanoprobing inside an SEM. The NW's electrical breakdown parameters (i.e., the breakdown voltage, power, and current density) were quantified, and their dependence on the NW diameter and the nanoprobing contact resistance (determined by the Si-doping level of the top n^+-GaN segment) was examined. By tuning the Si-doping concentration of the n^+-GaN segment, we achieved a NW breakdown current density of 4.65 MA/cm^2 and a breakdown power of 96.84 mW, both the highest among the previously reported results from GaN NWs. The results provide an experimental guideline on how to improve the electrical properties of GaN NWs grown on Si substrates for constructing high-performance electronics.

See supplementary material for details of the epitaxial growth of n-i-n-n^+ GaN NWs, e-beam deposition of Ti/Au electrodes, and doping-dependent curve of NW breakdown current density on the NW diameter.

The authors acknowledge the financial support from the Natural Sciences and Engineering Research Council of Canada (NSERC) (Grant Nos. STPGP-2014-463182, RGPIN-2017-06374, and EQPEQ-2015-72835), the Canada Research Chairs Program (Grant No. 237293), the Fonds de recherche du Québec - Nature et technologies (FRQNT) (through a Merit Scholarship to J. Qu), and the CMC Microsystems (through the Micro-Nano Technologies Financial Assistance Program).

[1] Y. Huang, X. Duan, Y. Cui, and C. M. Lieber, Nano Lett. **2**(2), 101 (2002).
[2] R. K. Debnath, R. Meijers, T. Richter, T. Stoica, R. Calarco, and H. Luth, Appl. Phys. Lett. **90**(12), 123117 (2007).
[3] D. Y. Jeon, K. H. Kim, S. J. Park, J. H. Huh, H. Y. Kim, C. Y. Yim, and G. T. Kim, Appl. Phys. Lett. **89**(2), 023108 (2006).
[4] T. Westover, R. Jones, J. Y. Huang, G. Wang, E. Lai, and A. A. Talin, Nano Lett. **9**(1), 257 (2009).
[5] J. Zhao, H. Sun, S. Dai, Y. Wang, and J. Zhu, Nano Lett. **11**(11), 4647 (2011).
[6] D. Li, Y. Wu, P. Kim, L. Shi, P. Yang, and A. Majumdar, Appl. Phys. Lett. **83**(14), 2934 (2003).
[7] L. H. Liang and B. Li, Phys. Rev. B **73**, 153303 (2006).
[8] K. Kishino, H. Sekiguchi, and A. Kikuchi, J. Cryst. Growth **311**(7), 2063 (2009).
[9] A. Bengoechea-Encabo, F. Barbagini, S. Fernandez-Garrido, J. Grandal, J. Ristic, M. Sanchez-Garcia, E. Calleja, U. Jahn, E. Luna, and A. Trampert, J. Cryst. Growth **325**(1), 89 (2011).
[10] H. Sekiguchi, K. Kishino, and A. Kikuchi, Appl. Phys. Express **1**(12), 124002 (2008).
[11] K. Kishino, K. Nagashima, and K. Yamano, Appl. Phys. Express **6**(1), 012101 (2013).
[12] H. Sekiguchi, K. Kishino, and A. Kikuchi, Appl. Phys. Lett. **96**(23), 231104 (2010).
[13] Y.-H. Ra, R. Wang, S. Y. Woo, M. Djavid, S. M. Sadaf, J. Lee, G. A. Botton, and Z. Mi, Nano Lett. **16**(7), 4608 (2016).
[14] K. A. Bertness, A. W. Sanders, D. M. Rourke, T. E. Harvey, A. Roshko, J. B. Schlager, and N. A. Sanford, Adv. Funct. Mater. **20**(17), 2911 (2010).
[15] T. Gotschke, T. Schumann, F. Limbach, T. Stoica, and R. Calarco, Appl. Phys. Lett. **98**(10), 103102 (2011).
[16] K. Kishino, T. Hoshino, S. Ishizawa, and A. Kikuchi, Electron. Lett. **44**(13), 819 (2008).
[17] R. Wang, Y.-H. Ra, Y. Wu, S. Zhao, H. P. T. Nguyen, I. Shih, and Z. Mi, Proc. SPIE **9748**, 97481S (2016).
[18] H. P. T. Nguyen, M. Djavid, S. Y. Woo, X. Liu, A. T. Connie, S. Sadaf, Q. Wang, G. A. Botton, I. Shih, and Z. Mi, Sci. Rep. **5**, 7744 (2015).
[19] J. Qu, M. Lee, M. Hilke, and X. Liu, Nanotechnology **28**(34), 345702 (2017).
[20] A. Vila, F. F. Hernändez-Ramirez, J. Rodrägeuz, O. Casals, A. Romano-Rodräguez, J. Morante, and M. Abid, Mater. Sci. Eng., C **26**(5), 1063 (2006).
[21] G. D. Marzi, D. Iacopino, A. J. Quinn, and G. Redmond, J. Appl. Phys. **96**(6), 3458 (2004).
[22] P. Mark and W. Helfrich, J. Appl. Phys. **33**(1), 205 (1962).
[23] A. Rose, Phys. Rev. **97**(6), 1538 (1955).
[24] S. Sze, *Physics of Semiconductor Devices* (Wiley, New York, 1969), p. 42.
[25] F. Schwierz, Solid State Electron. **49**(6), 889 (2005).
[26] J. Zhao, J.-Q. Huang, F. Wei, and J. Zhu, Nano Lett. **10**(11), 4309 (2010).
[27] F. A. Faria, J. Guo, P. Zhao, G. Li, P. K. Kandaswamy, M. Wistey, H. G. Xing, and D. Jena, Appl. Phys. Lett. **101**(3), 032109 (2012).
[28] S. I. Lopatin, V. L. Stolyarova, V. G. Sevast'yanov, P. Y. Nosatenko, V. V. Gorskii, D. V. Sevast'yanov, and N. T. Kuznetsov, Russ. J. Inorg. Chem. **57**(2), 219 (2012).
[29] J. V. Mantese and W. V. Alcini, J. Electron. Mater. **17**(4), 285 (1988).
[30] K. N. Chen, A. Fan, C. S. Tan, and R. Reif, IEEE Electron Device Lett. **25**(1), 10 (2004).
[31] G. E. Moore, IEEE J. Solid-State Circuits **11**(3), 33 (2006).
[32] G. E. Moore, IEEE J. Solid-State Circuits **11**(3), 36 (2006).